future pharmacology

MDPI

Article

Integrative Genomic and Structure-Based Prioritization of Molecular Targets in Multidrug-Resistant *Salmonella enterica* from Brazilian Poultry

Juan Philippe Teixeira [1,*], Daniel Ferreira de Lima Neto [1], Chiara Ascencio Brancalion [1], Miklos Maximiliano Bajay [1], Pedro Filipe de Souza Teles [2], Rafael Straus de Sá [1], Saad Khan [1], Thales Quedi Furian [3] and Lenita de Cássia Moura Stefani [2]

[1] Graduate Program in Biochemistry and Molecular Biology (PMBqBM), Center for Agricultural and Veterinary Sciences, State University of Santa Catarina, Lages 88520-000, SC, Brazil
[2] Graduate Program in Animal Science (PPGZOO), State University of Santa Catarina, Chapecó 89815-630, SC, Brazil
[3] Center for Diagnosis and Research in Avian Pathology (CDPA), Federal University of Rio Grande do Sul, Porto Alegre 91540-000, RS, Brazil
* Correspondence: juan.teixeira0863@edu.udesc.br

Abstract

Background/Objectives: Multidrug-resistant *Salmonella enterica* in poultry production poses a persistent challenge for antimicrobial stewardship and food safety. This study integrated phenotypic susceptibility testing, whole-genome sequencing, structural bioinformatics, molecular docking, and cheminformatics to prioritize resistance- and virulence-associated proteins in *S.* Heidelberg and *S.* Minnesota. **Methods:** Five multidrug-resistant poultry-associated isolates—SH16.3, SH23.6, SM23.7, SM23.8, and SM23.9—were analyzed. Resistome and virulome profiles guided the selection of CTX-M-2, CMY-2, Sul2, AcrB, and SpvC. Experimental protein structures or a high-confidence ColabFold model were used for GNINA docking. AcrB- and Sul2-directed analogs were generated with RDKit/BRICS and ranked by docking score, physicochemical properties, structural similarity, and PLIP interaction profile. **Results:** The SH23.6, SM23.7, SM23.8, and SM23.9 assemblies supported comparative genomic analysis, whereas SH16.3 was highly fragmented and restricted to target-level interpretation. Independent integrity checks recovered complete blaCTX-M-2 and spvC coding sequences with 100% coverage and identity to curated references, although their assignment to SH16.3 remains limited by the absence of raw-read and orthogonal confirmation. CMY-2, Sul2, SpvC, and AcrB showed 99.81–100% sequence identity and full coverage relative to the selected experimental structures. Sul2 analog generation did not surpass the best parental compounds. By contrast, several AcrB analogs achieved more favorable docking scores than the reference ligands. ACRB_BRICS_00124 yielded a GNINA score of −10.80 kcal/mol and formed six hydrogen bonds, three hydrophobic contacts, and one salt bridge. **Conclusions:** The integrated workflow identified AcrB as the most tractable molecular target and ACRB_BRICS_00124 as the leading candidate for subsequent molecular-dynamics simulations, synthetic-feasibility assessment, and experimental validation.

Keywords: *Salmonella*; antimicrobial resistance; whole-genome sequencing; efflux pump; molecular docking; cheminformatics

Check for updates

Academic Editors: George J. Kontoghiorghes and Malamati Kourti

Received: 26 June 2026
Revised: 10 September 2026
Accepted: 13 September 2026
Published: 30 September 2026

Copyright: © 2026 by the authors. Licensee MDPI, Basel, Switzerland. This article is an open access article distributed under the terms and conditions of the Creative Commons Attribution (CC BY) license.

1. Introduction

Nontyphoidal salmonellosis remains one of the leading foodborne bacterial zoonoses worldwide, causing gastroenteritis associated with the consumption of contaminated products, especially those of animal origin. Transmission frequently occurs through foods such as eggs, meat, and poultry products, making surveillance of this pathogen particularly important in intensive poultry production systems [1].

In Brazil, the poultry industry is of great economic and public health importance, and recent genomic studies show that certain serovars of *Salmonella enterica* are playing a prominent role in this sector. Among them, *Salmonella* Heidelberg and *S.* Minnesota have been described as prevalent or emerging serovars in Brazilian poultry production, with circulation also detected in exported products, reinforcing their potential impact on public health and international trade [2].

This situation is exacerbated by the spread of antimicrobial resistance. In Brazilian isolates of *S.* Heidelberg and *S.* Minnesota from poultry, resistance profiles to third-generation cephalosporins and fluoroquinolones have already been described, in addition to the presence of relevant genes such as blaCMY-2, associated with plasmid replicons, and sets of determinants linked to multidrug resistance and virulence [3]. In a more recent study of *S.* Heidelberg isolated from broiler chickens in Brazil, a high frequency of antimicrobial resistance and association with multiple resistance and virulence genes was observed, reinforcing the epidemiological potential of this serovar in the poultry industry [4].

Similarly, *S.* Minnesota has been recognized as an emerging serovar in Brazilian poultry farming. Recent data obtained from isolates derived from chicken litter in southern Brazil showed that samples of this serovar exhibited a multidrug-resistant profile confirmed both phenotypically and genetically, which supports concerns regarding its persistence and spread in the production environment [5]. Furthermore, analyses of environmental persistence and genotypic/phenotypic profiles indicate that *S.* Minnesota is frequently associated with the poultry production chain and with genes such as tetA and blaCMY-2, reinforcing its adaptation to this niche [6].

As a result, whole-genome sequencing (WGS) has become a key tool for the surveillance of foodborne pathogens. This approach allows for high-resolution characterization of the resistome, virulome, plasmidome, and genetic relationships among isolates, expanding the capacity for epidemiological tracking and interpretation of the mechanisms involved in antimicrobial resistance [7]. In Salmonella surveillance, WGS has also been adopted by food safety authorities and monitoring networks, precisely because of its value for typing, outbreak investigation, and genomic comparison among isolates from different sources [8].

However, the genomic identification of resistance and virulence genes, while essential, is not sufficient on its own to indicate which molecular targets hold the greatest potential for functional and pharmacological exploitation. Proteins such as β-lactamases, enzymes associated with sulfonamide resistance, and components of multidrug efflux systems constitute particularly relevant targets because they represent central mechanisms of bacterial survival under antimicrobial pressure. In the case of efflux pumps, there is recent evidence that systems such as AcrAB/AcrD in Salmonella remain important targets in in silico and experimental studies aimed at identifying inhibitors [9]. Comparative reassessment of AcrB efflux inhibitors further shows that inhibitor activity can depend on specific pump mutations [10].

Thus, approaches that integrate resistance phenotypes, comparative genomics, and structural prioritization through molecular modeling and docking can offer a rational strategy for transforming surveillance data into more refined mechanistic hypotheses. This integration allows for a reduction in redundancies, the selection of targets biologically consistent with the profile observed in the isolates, and, at the same time, the guidance of

the initial screening of ligands with the potential to interact with proteins associated with resistance and virulence. In light of this overview, the present study sought to characterize multidrug-resistant isolates of *S.* Heidelberg and *S.* Minnesota from the Brazilian poultry industry, integrating phenotypic, genomic, and structural data for the rational selection of molecular targets of interest. The overall workflow is summarized in Figure 1.

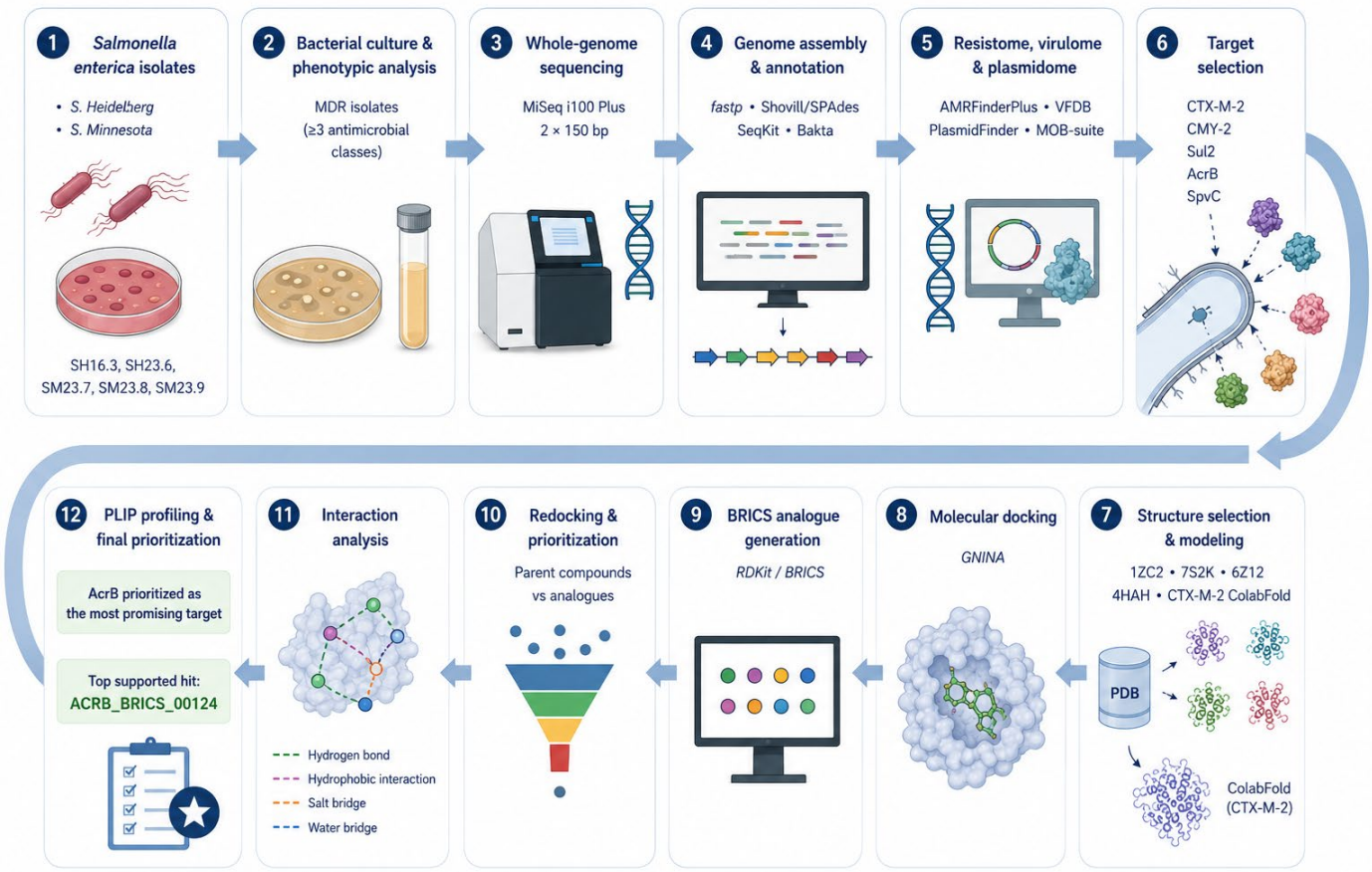


Figure 1. Integrated workflow for genomic characterization and structure-based prioritization of molecular targets. The workflow summarizes the analytical sequence from isolate selection and phenotypic characterization to genomic screening, target selection, docking, analog prioritization, interaction profiling, and final computational prioritization. Abbreviations: AcrB, acriflavine resistance protein B; BRICS, breaking of retrosynthetically interesting chemical substructures; CMY-2, class C beta-lactamase CMY-2; CTX-M-2, class A extended-spectrum beta-lactamase CTX-M-2; GNINA, deep-learning-assisted molecular docking software; MDR, multidrug resistance; PDB, Protein Data Bank; PLIP, Protein–Ligand Interaction Profiler; RDKit, open-source cheminformatics toolkit; SRA, Sequence Read Archive; Sul2, sulfonamide-resistant dihydropteroate synthase; WGS, whole-genome sequencing.

2. Materials and Methods

2.1. Selection of Strains, Origin of Isolates, Phenotypic Profile, and Criteria for Multidrug Resistance

The five Salmonella enterica isolates analyzed in this study were serotyped and supplied by the Center for Diagnosis and Research in Avian Pathology (CDPA), Federal University of Rio Grande do Sul (UFRGS), Porto Alegre, RS, Brazil. The study included SH16.3, SH23.6, SM23.7, SM23.8, and SM23.9, representing *S.* Heidelberg and *S.* Minnesota isolates collected in 2016 and 2023. The isolate identifiers used throughout the manuscript correspond to internal strain codes; public sequence accession numbers will be added to the Data Availability Statement after completion of Sequence Read Archive deposition.

According to the available metadata, all isolates originated from swab samples collected within Brazilian poultry-production facilities; SM23.7 and SM23.9 were drag-swab isolates from commercial broiler houses. The collection states were Santa Catarina for SH16.3, Rio Grande do Sul for SH23.6 and SM23.8, and Paraná for SM23.7 and SM23.9. Company, farm, and municipality names were withheld because authorization for public disclosure was not available. All five isolates fulfilled the multidrug-resistance definition of resistance to three or more antimicrobial classes [11].

The primary susceptibility profile was used for MDR eligibility and phenotype–genotype interpretation. A separate complementary antimicrobial-susceptibility assay was performed by Mercolab Laboratórios Ltd.a. (Chapecó, SC, Brazil) on the 2023 isolates SH23.6, SM23.7, SM23.8, and SM23.9. Samples were submitted on 6 April 2026 and the results were issued on 9 April 2026. The laboratory recorded the material as drag swabs of poultry litter and used the disk-diffusion method. The panel comprised amoxicillin, ampicillin, cefalexin, ceftiofur, cefoxitin, ciprofloxacin, colistin, doxycycline, enrofloxacin, fosfomycin, gentamicin, lincomycin, marbofloxacin, neomycin, norfloxacin, penicillin, polymyxin B, sulfadiazine-trimethoprim, sulfamethoxazole-trimethoprim, tetracycline, tiamulin, tilmicosin, and tulathromycin. The official report classified the results as susceptible, intermediate, or resistant under the laboratory procedure POP B09 and cited CLSI M31-A3 (2008). Because inhibition-zone diameters, replicate counts, and the quality-control strain were not reported, the issued classifications were transcribed without reinterpretation and were used only as complementary descriptive evidence; they were not used to establish MDR eligibility.

2.2. Bacterial Reactivation, Culture Preparation, and Genomic DNA Extraction

Brain Heart Infusion (BHI), Rappaport–Vassiliadis, and XLD (Xylose-Lysine-Deoxycholate Agar) media were prepared according to the manufacturers' recommendations and pre-incubated at 37 °C for 24 h to verify sterility and microbiological quality. Each *Salmonella* spp. isolate was initially inoculated into 5 mL of BHI and incubated at 37 °C for 24 h. Subsequently, a 1 mL aliquot of the culture was transferred to 5 mL of Rappaport–Vassiliadis medium, with additional incubation for 24 h at 37 °C. After selective enrichment, aliquots of the cultures were seeded onto plates containing XLD medium. From the resulting growth, a single colony was selected, reinoculated into BHI, and incubated for an additional 24 h at 37 °C. Genomic DNA was extracted and purified using the PureLink™ kit (Thermo Fisher Scientific, Carlsbad, CA, USA), following the manufacturer's instructions. Following enzymatic digestion with proteinase K, a modification was included in the protocol, consisting of an additional step of mechanical lysis via 10 consecutive pipetting movements ("up and down") for each sample, with the aim of increasing the efficiency of bacterial genetic material release.

2.3. Qualitative and Quantitative DNA Assessment

The integrity of the extracted DNA was assessed by 0.8% agarose gel electrophoresis with ethidium bromide, using 10 µL of each sample, based on an established molecular cloning protocol [12], with minor adaptations. This step was used to verify the molecular integrity and apparent size of the extracted genomic DNA. DNA purity was assessed by spectrophotometry using a NanoDrop™ instrument (Thermo Fisher Scientific, Waltham, MA, USA), with 1.5 µL of each sample deposited directly onto the instrument's sample well. The A260/280 ratio was used primarily as an indicator of protein carryover or other contaminants absorbing near 280 nm, whereas the A260/230 ratio was used as an indicator of residual salts, phenols, guanidine, carbohydrates, or other extraction-related contaminants. Values close to 1.8–2.0 for A260/280 and 2.0–2.2 for A260/230 were adopted

as quality thresholds for downstream library preparation [13]. Absolute DNA quantification was performed by fluorometry using a Qubit™ 4 fluorometer (Invitrogen, Carlsbad, CA, USA), with a specific kit for dsDNA. The concentrations obtained were used to adjust the samples before genomic-library preparation. After preparation, sequencing libraries were normalized to a final molar concentration of 10 nM.

2.4. Library Preparation and Whole-Genome Sequencing

Sequencing libraries were prepared using the Illumina DNA Prep kit (Illumina, Inc., San Diego, CA, USA) according to the manufacturer's protocol. The five isolates were sequenced on the MiSeq i100 Plus platform (Illumina, San Diego, CA, USA) using a 2 × 150 bp paired-end strategy with the MiSeq™ i100 Series Dry Cartridge 600 Cycles–5M (Illumina, Inc., San Diego, CA, USA). The sequencing yield was compatible with an estimated minimum coverage of 30× per isolate.

2.5. Preprocessing of Reads, Reassembly, and Genomic Quality Assessment

Raw sequencing reads underwent quality control with fastp (https://github.com/OpenGene/fastp; accessed on 12 September 2026), which removed adapters, trimmed bases with a quality score below Q30, and discarded reads shorter than 50 bp [14]. The reports generated in HTML and JSON formats were individually inspected for overall quality, GC content, duplication rate, and read size distribution. De novo assembly was performed using SPAdes v3.15 via the Shovill v1.1.0 pipeline, which integrates read filtering, read organization, and optimized assembly for bacterial genomes [15]. Each sample generated two main files: spades.fasta, containing the raw contigs, and contigs.fa, containing the filtered contigs with a length $\geq$ 500 bp. Successful completion of assembly was confirmed by reviewing the SPAdes log files. The assembly graphs (contigs.gfa) were preserved for visual inspection in Bandage [16]. Assembly quality metrics were obtained using SeqKit v2.8.0, which was used to calculate the number of contigs, total genome size, longest contig, N50, L50, and GC content for each sample [17]. Comparison between the raw and filtered files showed that the removal of short contigs did not substantially alter the overall architecture of the assemblies, indicating the stability of the genome reconstruction process.

Assembly quality was evaluated using genome size, contig count, N50, longest contig, and GC content. SH16.3 was classified as a fragmented assembly and was excluded from genome-wide comparative analyses. Its *blaCTX-M-2* and *spvC* sequences were retained for target-level structural assessment, while the four remaining assemblies were used for comparative genomic interpretation.

Because SH16.3 was highly fragmented, *blaCTX-M-2* and *spvC* underwent independent target-level checks using AMRFinderPlus v4.2.7 (database version 2026-05-15.1), Prodigal v2.6.3 [18], and ABRicate v1.4.0 against VFDB (release 3 April 2026) [19,20]. Coverage, identity, ORF completeness, contig-end distance, and alignment gaps were evaluated; the absence of raw reads and orthogonal laboratory confirmation was retained as a limitation.

2.6. Identification of the Genetic Determinants of Resistance, Virulence, Biofilm Formation, and Persistence

The genotypic characterization integrated databases for antimicrobial resistance, virulence, and mobile genetic elements. Antimicrobial-resistance determinants were screened using AMRFinderPlus, CARD, ResFinder, ARG-ANNOT, and MEGARes [19,21–24]. Virulence factors were screened against VFDB [20], and plasmid characterization used PlasmidFinder (https://cge.food.dtu.dk/services/PlasmidFinder/; accessed on 12 September 2026) with MOB-suite (https://github.com/phac-nml/mob-suite; accessed on 12 September 2026) reconstruction/typing [25,26]. AMRFinderPlus v3.12.8 was run with database version 2024-07-22.1, and ABRicate was used against CARD, ResFinder, ARG-ANNOT, MEGARes,

VFDB, PlasmidFinder, Ecoh, Ecoli_VF, BacMet2, and NCBI databases. BacMet2 protein-level searches were performed with DIAMOND blastp (https://github.com/bbuchfink/diamond; accessed on 12 September 2026) [27] against the BacMet database [28]. Biofilm and adhesion genes were organized into curated biological modules. Outputs were consolidated using custom scripts to produce presence/absence matrices and functional panels.

2.7. Sample Selection for the Structural Phase and Genotype–Phenotype Correlation

Target eligibility was evaluated using an explicit rule-based decision process rather than a retrospective weighted score. A candidate was advanced when it satisfied the following conditions: (i) a direct mechanistic relationship with the observed resistance phenotype or a clearly defined catalytic virulence mechanism; (ii) recovery of a complete or interpretable coding sequence; (iii) adequate correspondence to an experimental structure or a high-confidence predictive model; (iv) availability of a biologically defensible binding region and target-directed ligand set; and (v) non-redundancy with another protein representing the same analytical question. Identical protein sequences across isolates were collapsed to a single representative. The resulting decisions are summarized in Table 1.

Table 1. Explicit target-eligibility decision matrix used for the structural phase.

Candidate	Primary Biological Link	Structural/Site Evidence	Decision	Operational Rationale
CTX-M-2	Extended-spectrum β-lactam resistance	High-confidence ColabFold model; catalytic motifs preserved	Target-level inclusion	Mechanistically relevant ESBL target with a high-confidence structural model.
CMY-2	AmpC-mediated cephalosporin resistance	PDB 1ZC2; 100% identity and coverage	Reference docking	Complete experimental receptor correspondence and target-directed β-lactam library.
Sul2	Sulfonamide resistance/folate pathway	PDB 7S2K; 100% identity and coverage; Mg^{2+}-dependent site	Docking + analog generation	Conserved target, defined site, coherent sulfonamide/PABA chemical series.
AcrB	Multidrug efflux	PDB 6Z12; 99.81% identity; distal pocket/hydrophobic trap	Docking + analog generation	Conserved in four isolates, well-defined pocket, diverse validated substrate/inhibitor seeds.
SpvC	Catalytic virulence effector	PDB 4HAH; 100% identity and coverage	Target-level exploratory docking	Catalytic virulence effector with an experimental structure and a defined active site.
Tet(A)	Tetracycline efflux	Integral membrane antiporter; no target-specific pocket protocol established	Not advanced	Would require a membrane-aware, target-specific workflow; efflux was already represented by structurally tractable AcrB.
InvA	Conserved invasion machinery	Conserved marker, but not directly explanatory of the MDR phenotype	Not advanced	Useful for identification/virulence context, but outside the resistance-focused structural question and ligand-library design.

2.8. Structural Annotation, Extraction of Target Proteins, and Sequence Validation

The genomes selected for the structural stage were annotated using Bakta (https://github.com/oschwengers/bakta; accessed on 12 September 2026), with a complete local database and multithreaded processing, to generate standardized annotation files in FAA, FFN, GFF3, GBFF, and TSV formats [29]. From the tabular and amino acid files, proteins annotated as β-lactamases, efflux transporters, folate metabolism enzymes, and virulence factors were retrieved. The extracted sequences of interest were compared for length and identity across the selected samples, allowing us to confirm redundancies and identify more representative variants. Next, for each structural target, the sequence derived from the genome was compared to the sequence present in the selected experimental structures in the Protein Data Bank (PDB), ensuring adequate coverage and alignment for docking.

2.9. Selection and Preparation of Experimental Three-Dimensional Structures

For targets with suitable experimental three-dimensional structures, the entries 1ZC2 (CMY-2), 7S2K (Sul2), 6Z12 (AcrB), and 4HAH (SpvC) were selected from the Protein Data Bank. The structures were chosen based on functional correspondence, sequence coverage, and suitability for molecular screening. The chains of interest were extracted using custom Python scripts, and water molecules and non-essential heteroatoms were removed. For Sul2, the crystallographic Mg^{2+} ion in 7S2K was documented as part of the functional-site context, and receptor preparation was inspected with and without this cofactor to avoid artifactual interpretation of the binding site. For CMY-2, AcrB, and SpvC, cleaned versions of the selected chain were used.

2.10. Structural Modeling of CTX-M-2

The CTX-M-2 target, derived from isolate SH16.3, underwent structural modeling using ColabFold v1.6.0 in a GPU-accelerated Linux environment, employing automatic templates, homology search via MMseqs2 (https://github.com/soedinglab/MMseqs2; accessed on 12 September 2026), and final Amber relaxation as implemented in ColabFold v1.6.0 [30,31]. The best model was selected based on the pipeline's internal ranking. After modeling, the conserved catalytic motifs characteristic of class A β-lactamases were examined, including the SXXK motif, the SDN motif, and the KTG motif, which were used as a complementary check of the structural and functional consistency of the selected model. These residues were also used as a reference for positioning the docking box.

2.11. Construction of Chemical Libraries and Preparation of Linkers

The ligand libraries were assembled in a target-directed manner and retrieved from PubChem in SDF format using a custom Python script [32]. For Sul2, classical sulfonamides and compounds related to the PABA/folate pathway were tested; for CMY-2 and CTX-M-2, a panel of β-lactams and β-lactamase inhibitors was used; for AcrB, classic substrates and inhibitors of efflux pumps were included; and for SpvC, an exploratory set of phosphorylated and phosphonated compounds was used. The molecules were organized into target-specific subsets, preserving pharmacological consistency between the biological mechanism and the chemical library employed.

2.12. Molecular Docking of Reference Compounds

Molecular docking was performed with GNINA v1.0 [33,34], which uses a Vina-derived search and scoring framework together with convolutional-neural-network pose assessment and rescoring. For CMY-2 and Sul2, ligand-guided autoboxing was based on co-crystallized ligands. AcrB docking targeted the distal pocket/hydrophobic trap, SpvC docking targeted the catalytic cavity, and the CTX-M-2 box was centered on the conserved

catalytic motifs. Receptor coordinates, docking-box dimensions, exhaustiveness, and mode counts were maintained within each target-specific campaign. Compounds were ranked by GNINA score and pose quality.

2.13. Analog Generation, Cheminformatics-Based Prioritization, and Redocking

Computational analog generation was conducted with RDKit release 2024.09.2 [35] using BRICS fragmentation/recombination rules [36]. Parent molecules were sanitized, canonicalized, fragmented, recombined to a maximum depth of 2, deduplicated by canonical SMILES, embedded in three dimensions, and minimized with UFF [37]. AcrB seeds comprised minocycline, doxycycline, tetracycline, tigecycline, and phenylalanine-arginine β-naphthylamide (PAβN). Sul2 seeds comprised the best-ranked sulfonamide/PABA-pathway compounds. The generated compounds are computational structures only; no synthesis, chemical stability, or biological activity was established.

The cheminformatics-based prioritization of analogs was performed by calculating structural descriptors in RDKit, including molecular weight (MolWt), exact mass, cLogP, TPSA, number of hydrogen acceptors and donors, number of rotatable bonds, number of rings, number of heavy atoms, and formal charge. The QED (quantitative estimate of drug-likeness) index was also calculated, which is a metric proposed to rank compounds based on a trade-off between desirable physicochemical properties in bioactive molecules [38]. In addition, Morgan-type circular fingerprints were generated, and the Tanimoto similarity between each analog and the seed molecules was calculated.

The internal screening of the analogs was based on operational criteria defined for the campaign, requiring a molecular weight between 250 and 950 Da, cLogP between −1.5 and 7.5, TPSA between 40 and 260 $Å^2$, at least 2 rings, a maximum of 2 violations of drug-likeness rules, and a minimum similarity of 0.35 relative to the best seed molecule. Next, an internal PriorityScore was calculated by combining structural similarity, QED, penalty for violations, molecular weight proximity, and TPSA proximity, to rank the analogs and select candidates for redocking. The prioritized analogs were then redocked at the same molecular site used in the primary campaigns, preserving the receptor, box coordinates, number of modes, and exhaustiveness, in order to allow direct comparison between parent compounds and derivatives within a consistent protocol.

Only AcrB and Sul2 were advanced to BRICS analog generation because both combined a defined binding region with a coherent and sufficiently populated parent chemical series. CTX-M-2 and CMY-2 were not included in this stage because β-lactam recognition depends on scaffold integrity and catalytic chemistry that are not adequately represented by generic fragment recombination. SpvC was not advanced because its phosphorylated and phosphonated seed set was small and highly polar.

2.14. Analysis of Protein–Ligand Interactions and Final Prioritization of Complexes

Protein–ligand interactions were characterized with PLIP v3.0.0 [39], including hydrogen bonds, hydrophobic contacts, π-stacking, cation–π interactions, salt bridges, halogen bonds, metal interactions, and water bridges. Final prioritization integrated GNINA scores, pose geometry, PLIP interaction profiles, and cheminformatics descriptors. Compounds combining favorable docking scores with consistent pocket interactions were advanced as the leading candidates.

2.15. Data Visualization and Figure Generation

Data organization and graphical visualization were performed using custom Python scripts. Phenotypic resistance profiles, gene presence/absence matrices, assembly metrics, docking scores, analog-prioritization results, and PLIP interaction counts were organized

as pandas data frames, while NumPy supported numerical handling, matrix construction, categorical encoding, and graphical positioning.

Matplotlib was used to generate categorical heatmaps, horizontal bar charts, grouped interaction plots, and the analog-screening funnel. Discrete color maps were generated with matplotlib.colors.ListedColormap, and custom legend elements were produced with matplotlib.patches.Patch. Figure panels, labels, legends, and spacing were assembled programmatically.

Docking scores and interaction counts were plotted directly from the processed tables. The revised figures were generated using Python v3.13.12, pandas v3.0.5, NumPy v2.5.1, and Matplotlib v3.11.1 and exported as 600 dpi PNG files and vector PDF files using bbox_inches = "tight".

Figure 1 was independently designed and assembled by the authors to summarize the analytical workflow. Figures 2–9 were generated programmatically. Two-dimensional chemical structures were rendered with RDKit v2025.09.5 from validated canonical or isomeric SMILES and inspected before figure assembly.

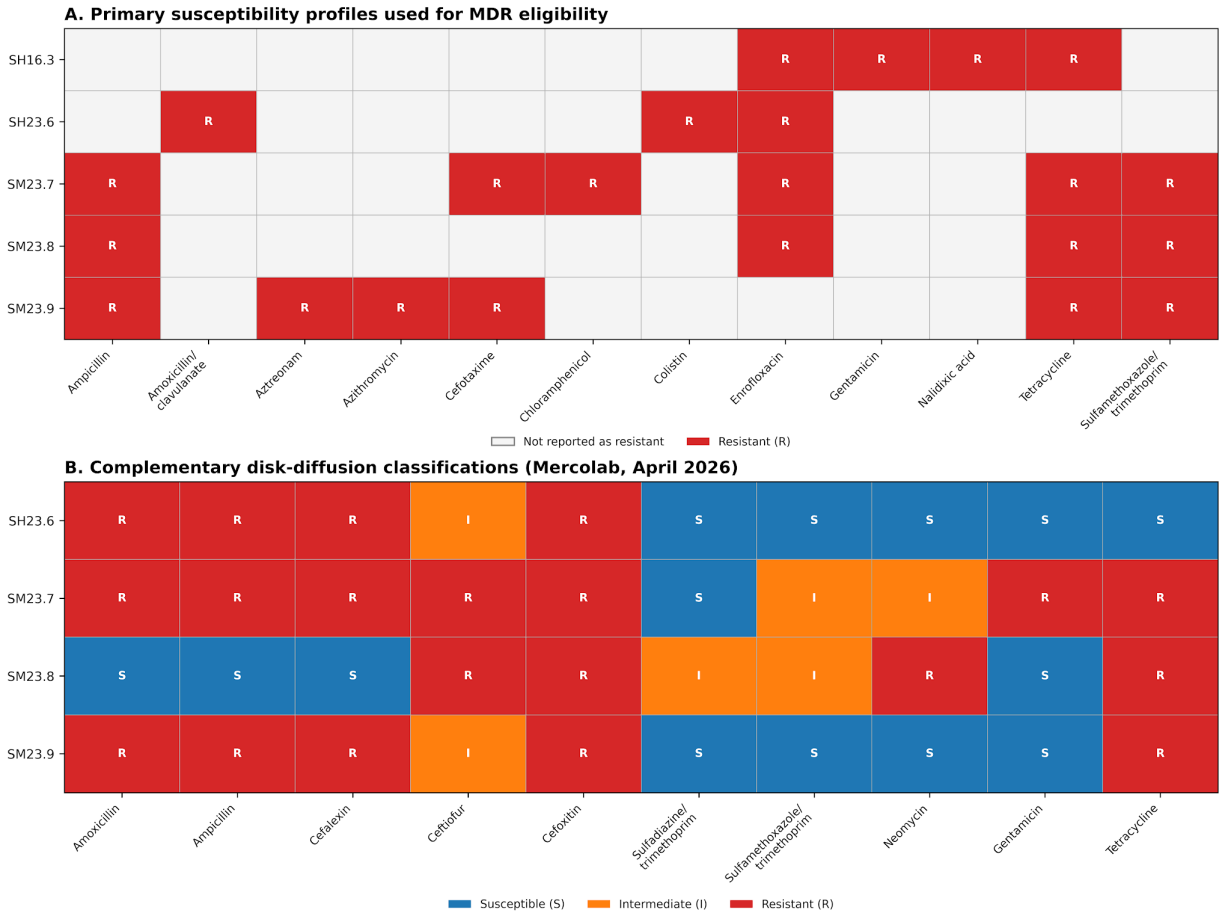


Figure 2. Phenotypic antimicrobial-susceptibility profiles. (**A**) Primary profiles used for MDR eligibility. (**B**) Complementary Mercolab disk-diffusion classifications (April 2026). S, susceptible; I, intermediate; R, resistant. Categories were transcribed without reinterpretation because inhibition-zone diameters were unavailable.

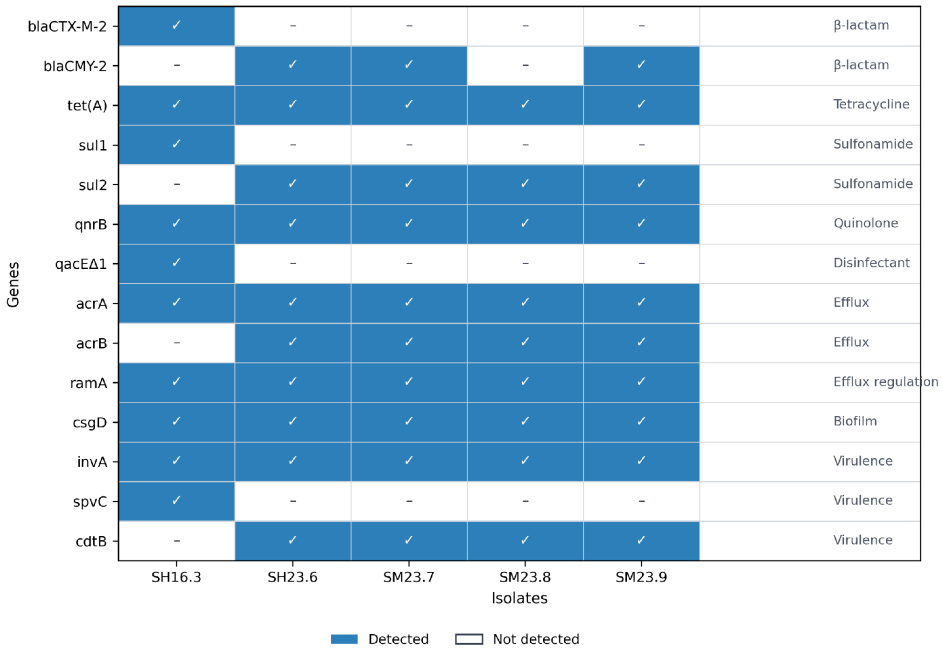


Figure 3. Presence/absence matrix of selected resistance, efflux, biofilm, and virulence-associated genes used in genotype–phenotype interpretation and target eligibility assessment.

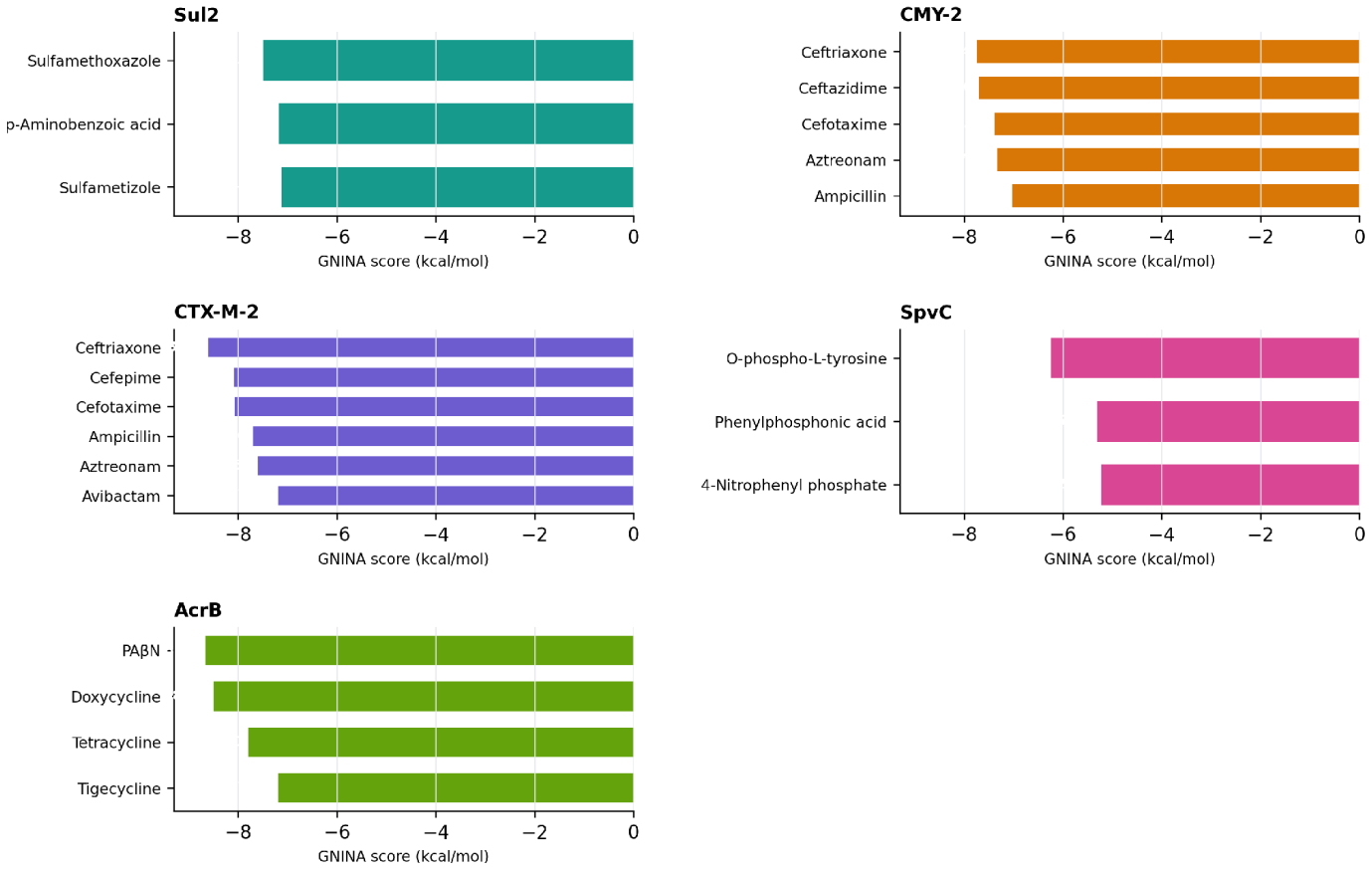


Figure 4. Target-specific GNINA docking scores for the reference compounds evaluated against Sul2, CMY-2, CTX-M-2, SpvC, and AcrB.

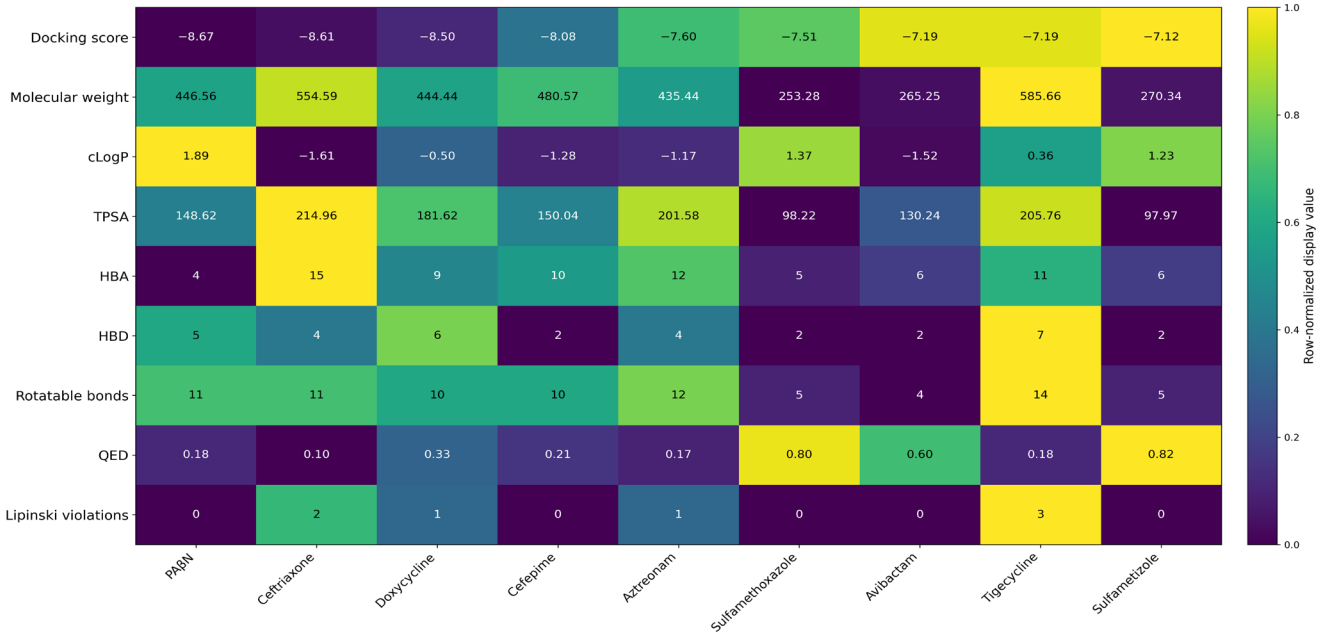


Figure 5. Physicochemical descriptors and docking scores for representative compounds. Numerical values are displayed directly; color scaling is normalized separately within each descriptor row and is used only to aid visual comparison.

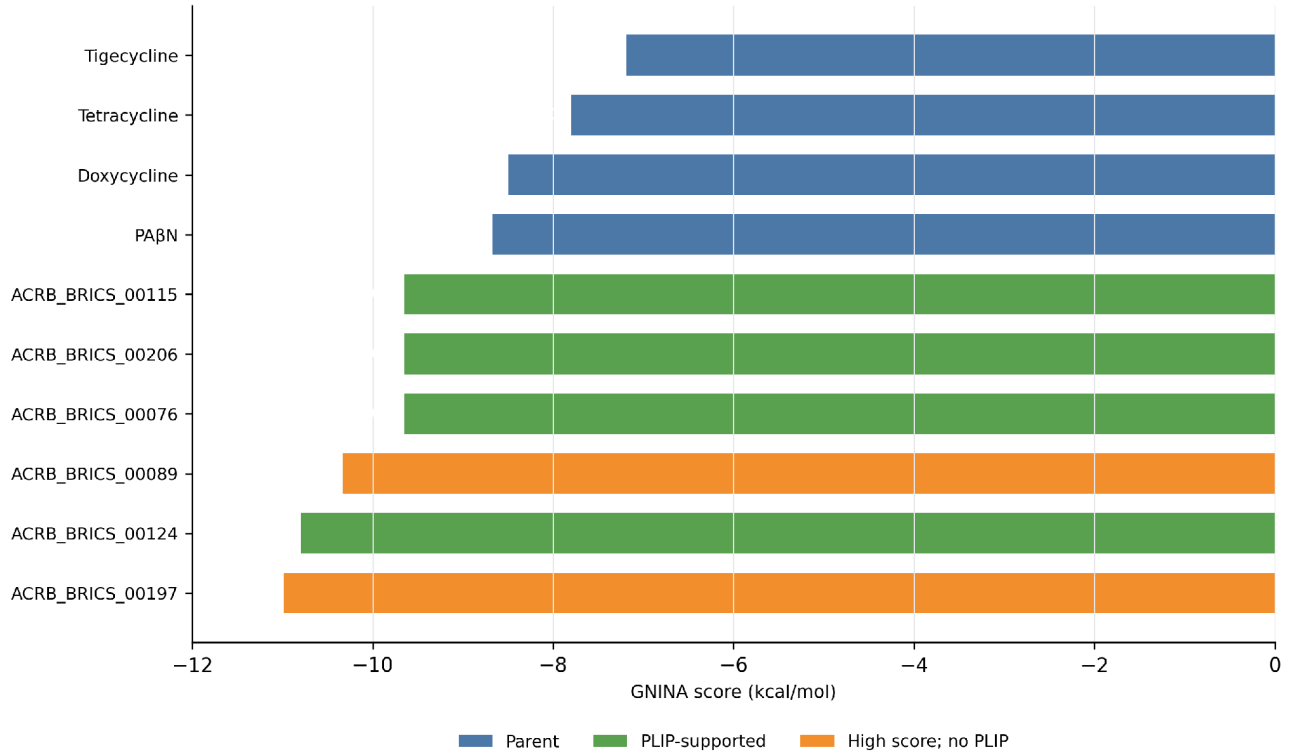


Figure 6. Comparison of reference parent compounds and top AcrB BRICS-derived analogs. Green bars denote candidates with explicit PLIP-supported contacts; orange bars denote high-scoring poses for which PLIP did not recover explicit contacts; blue bars denote parent compounds.

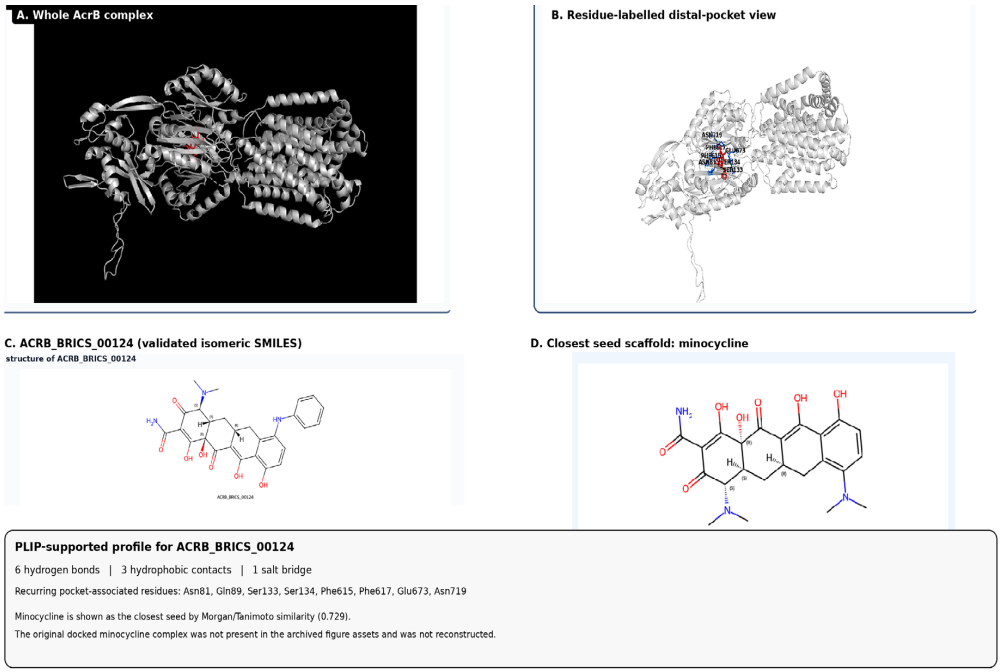


Figure 7. AcrB distal-pocket visualization and chemical context. Panel (**A**) shows the complete AcrB–ACRB_BRICS_00124 complex; panel (**B**) enlarges the residue-labeled distal pocket retained from the archived interaction output; panel (**C**) shows the validated two-dimensional structure of ACRB_BRICS_00124; and panel (**D**) shows minocycline, the closest seed scaffold by Morgan/Tanimoto similarity. The integrated PLIP profile for ACRB_BRICS_00124 comprises six hydrogen bonds, three hydrophobic contacts, and one salt bridge. The original docked minocycline complex was not present in the archived figure assets and therefore was not reconstructed. Color coding: in the chemical depictions, oxygen atoms are shown in red and nitrogen atoms in blue, while carbon frameworks are shown in black; the protein representation is shown in grayscale with pocket/ligand highlights retained from the interaction output.

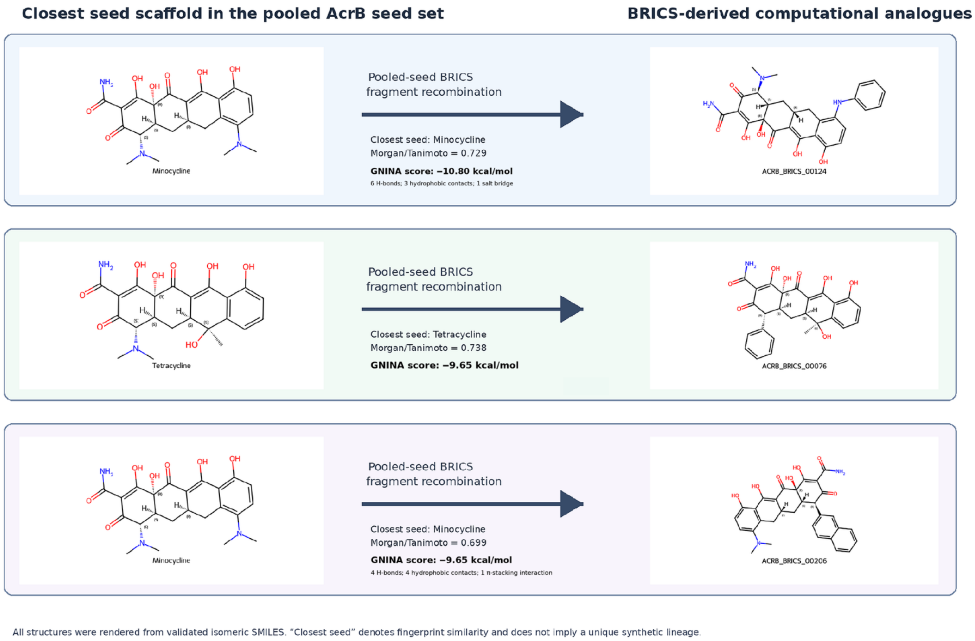


Figure 8. High-resolution chemical structures of the closest seed scaffolds and three interaction-supported AcrB analogs. Seed similarity was assigned using Morgan fingerprints and Tanimoto similarity within the pooled AcrB seed set. All structures were rendered from validated isomeric SMILES using RDKit. Background panel colors are used only to separate compound comparisons visually; atom colors follow the RDKit chemical depiction convention (oxygen red, nitrogen blue, carbon/bonds black).

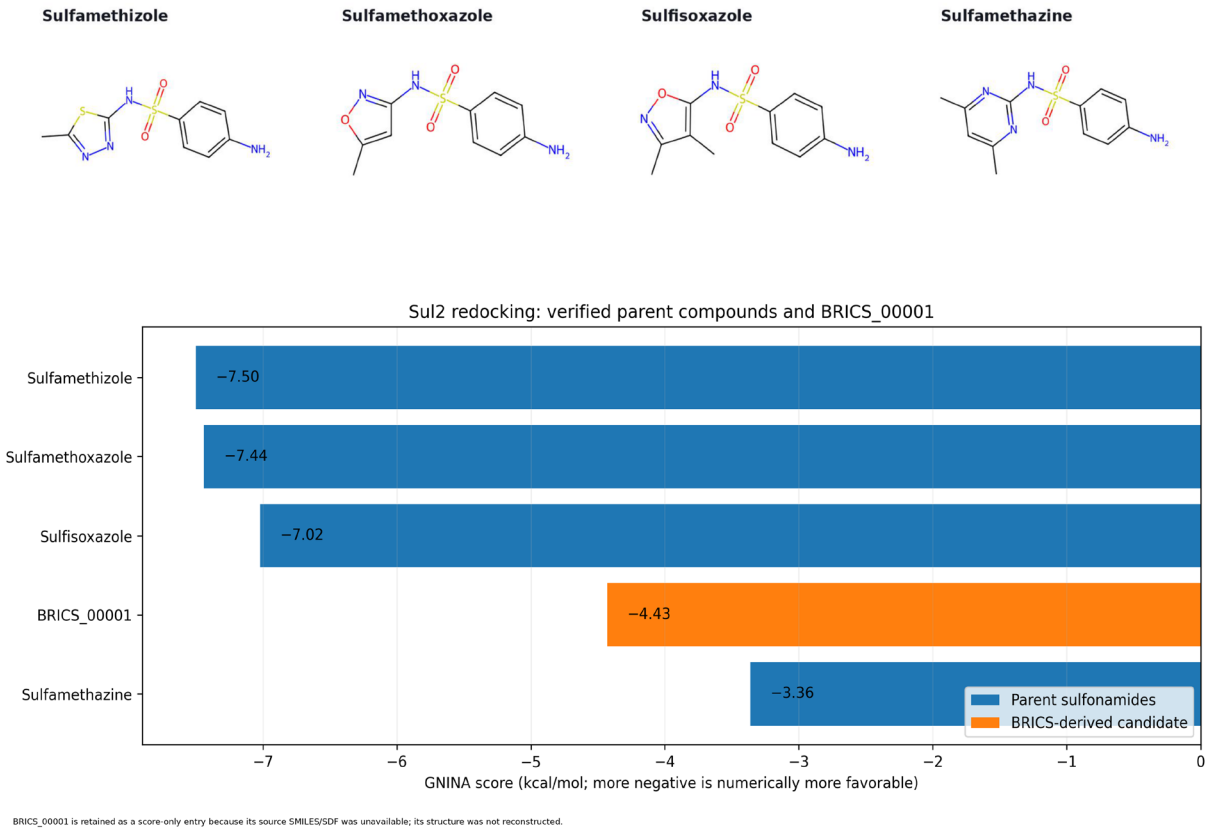


Figure 9. Verified parent-compound structures and GNINA redocking scores for the prioritized Sul2 set. Sulfamethizole, sulfamethoxazole, sulfisoxazole, and sulfamethazine were rendered from verified canonical SMILES using RDKit. BRICS_00001 is retained in the score comparison; its exact structure is not depicted because the corresponding source SMILES/SDF was not present in the archived assets available for revision. In the score comparison, the BRICS-derived candidate is visually distinguished from the parent sulfonamides; the distinction is categorical only and does not encode an additional quantitative variable.

3. Results

3.1. Phenotypic Profile and Selection Rationale for the Strains

The five *Salmonella enterica* isolates included in the study had previously been classified as multidrug-resistant based on antibiotic susceptibility testing, as they exhibited resistance to three or more classes of antimicrobials [11]. This result provided the experimental starting point for subsequent genomic and structural investigations, as it indicated the presence of potentially multiple resistance mechanisms, combining enzymatic determinants, efflux systems, regulatory alterations, and possibly mobile elements associated with horizontal gene acquisition. Among the observed phenotypic profiles, SH16.3 exhibited resistance to gentamicin, enrofloxacin, nalidixic acid, and tetracycline, while SH23.6 showed resistance to colistin, amoxicillin/clavulanic acid, and enrofloxacin.

In contrast, the primary susceptibility profiles of the *S.* Minnesota isolates were broader. SM23.7 was resistant to ampicillin, chloramphenicol, cefotaxime, tetracycline, enrofloxacin, and sulfamethoxazole-trimethoprim; SM23.8 was resistant to ampicillin, tetracycline, enrofloxacin, and sulfamethoxazole-trimethoprim; and SM23.9 was resistant to ampicillin, aztreonam, cefotaxime, tetracycline, azithromycin, and sulfamethoxazole-trimethoprim. Together with the SH16.3 and SH23.6 profiles, these data supported the selection of isolates representing different combinations of resistance to beta-lactams, sulfonamides, tetracyclines, quinolones/fluoroquinolones, phenicols, aminoglycosides, and polymyxins. The isolate-level primary resistance profiles and MDR-class rationale are summarized in Table 2.

Table 2. Selected Salmonella enterica isolates, primary phenotypic resistance profiles, and MDR-class rationale used for downstream genomic and structural prioritization.

Isolate	Serovar/Year	Origin	Phenotypic Resistance Profile	Major MDR Classes Represented
SH16.3	*S.* Heidelberg/2016	Swab from a poultry-production facility; SC, Brazil	Gentamicin; enrofloxacin; nalidixic acid; tetracycline	Aminoglycoside; quinolone/fluoroquinolone; tetracycline
SH23.6	*S.* Heidelberg/2023	Swab from a poultry-production facility; RS, Brazil	Colistin; amoxicillin/clavulanic acid; enrofloxacin	Polymyxin; β-lactam/β-lactamase inhibitor; fluoroquinolone
SM23.7	*S.* Minnesota/2023	Drag swab from a commercial broiler house; PR, Brazil	Ampicillin; chloramphenicol; cefotaxime; tetracycline; enrofloxacin; sulfamethoxazole-trimethoprim	β-lactam; phenicol; tetracycline; fluoroquinolone; folate-pathway inhibitor
SM23.8	*S.* Minnesota/2023	Swab from a poultry-production facility; RS, Brazil	Ampicillin; tetracycline; enrofloxacin; sulfamethoxazole-trimethoprim	β-lactam; tetracycline; fluoroquinolone; folate-pathway inhibitor
SM23.9	*S.* Minnesota/2023	Drag swab from a commercial broiler house; PR, Brazil	Ampicillin; aztreonam; cefotaxime; tetracycline; azithromycin; sulfamethoxazole-trimethoprim	β-lactam; tetracycline; macrolide; folate-pathway inhibitor

The complementary assay yielded internally heterogeneous classifications and corrected the preliminary summary of the additional beta-lactam results. SH23.6 was resistant to amoxicillin and intermediate to ceftiofur; SM23.7 was resistant to both compounds; SM23.8 was susceptible to amoxicillin but resistant to ceftiofur; and SM23.9 was resistant to amoxicillin and intermediate to ceftiofur. The assay tested amoxicillin alone, not amoxicillin-clavulanate. Sulfonamide-trimethoprim and aminoglycoside classifications also varied: SH23.6 and SM23.9 were susceptible to both sulfonamide combinations, neomycin, and gentamicin; SM23.7 was intermediate to sulfamethoxazole-trimethoprim and neomycin and resistant to gentamicin; and SM23.8 was intermediate to both sulfonamide combinations, resistant to neomycin, and susceptible to gentamicin. These complementary categories are shown in Figure 2B and are interpreted descriptively.

3.2. Sequencing, Genome Assembly, and Assembly Quality

S. enterica. In contrast, SH16.3 was a marked technical outlier: 6.42 Mb, 4432 contigs, N50 of 4160 bp, largest contig of 83,346 bp, and a GC content of 51.79%. The available data do not distinguish among contamination, mixed culture, uneven coverage, repetitive/mobile-element content, or other technical/biological causes. Accordingly, no claim of increased biological complexity is made, and genome-wide interpretation was restricted. Independent target-level reanalysis identified *blaCTX-M-2* on contig00006 with 100% reference coverage and 100% identity in both nucleotide- and protein-level AMRFinderPlus analyses. The corresponding Prodigal CDS was complete (partial = 00) and located more than 8.9 kb from the nearest contig boundary. *spvC* was identified on the 1137 bp contig01213 with 726/726 nt coverage, 100% identity, no gaps, and a complete Prodigal CDS (partial = 00). These findings support coding-sequence integrity but do not resolve

isolate-level provenance without raw-read mapping or orthogonal confirmation. Assembly metrics are reported in Table 3.

Table 3. Genome-assembly metrics and interpretation used to delimit downstream genomic inference.

Isolate	Genome Size (bp)	Contigs ≥ 500 bp	N50 (bp)	Largest Contig (bp)	GC (%)	Interpretation
SH16.3	6,416,937	4432	4160	83,346	51.79	Fragmented; excluded genome-wide. Target-level integrity supported for blaCTX-M-2 and spvC.
SH23.6	4,920,696	93	271,377	615,915	52.14	Suitable for comparative genomic analysis.
SM23.7	4,784,913	83	271,306	693,633	52.22	Suitable for comparative genomic analysis.
SM23.8	4,794,223	97	248,432	694,302	52.21	Suitable for comparative genomic analysis.
SM23.9	4,889,021	111	225,578	648,334	52.11	Suitable for comparative genomic analysis.

3.3. Resistome, Virulome, and Consistency with the Observed Phenotype

Functional annotation and targeted screening revealed a resistance pattern that was biologically consistent with the previously observed multidrug-resistant antibiotic susceptibility profile. Among the five genomes analyzed, two main profiles stood out. The first was represented by strain SH16.3, in which blaCTX-M-2, sul1, tet(A), qacE/qacEdelta1, and the virulence factor spvC were identified. This set is consistent with a complex phenotype, involving resistance to extended-spectrum β-lactams, sulfonamides, and tetracyclines, as well as possible increased tolerance to quaternary ammonium compounds. The simultaneous presence of blaCTX-M-2 and spvC was particularly relevant, as it brought together in a single isolate a clinical resistance determinant and a virulence effector associated with bacterial survival and modulation of host–microbe interaction. The second profile was observed mainly in strains SH23.6, SM23.7, SM23.8, and SM23.9, in which the recurrent combination of acrB, sul2, and tet(A) was detected, accompanied, in part of the group, by genes from the CMY family. In SH23.6 and SM23.7, the presence of blaCMY-2 was clear and structurally consistent; in SM23.9, a member of the CMY family was detected, though with a reduced length compared to canonical CMY-2, whereas in SM23.8, the profile was dominated by AcrB, Sul2, and TetA, with no equally clear hit for CMY-2 in the regions prioritized for modeling. This pattern reinforces the idea that the resistance observed experimentally did not depend on a single mechanism, but rather on a functional arrangement combining enzymatic inactivation, active drug efflux, and classic determinants of acquired resistance. In interpretive terms, the association between tet(A), sul1/sul2, and β-lactamase genes offers a qualitatively consistent explanation for the low susceptibility to tetracyclines, sulfonamides, and β-lactams observed in multidrug-resistant strains. Concurrently, the presence of acrB, ramA, acrA, acrR, and other components of efflux systems suggests an additional layer of tolerance to multiple compounds, consistent with broader phenotypic profiles and persistence under antimicrobial pressure. Regarding virulence and persistence, the functional matrix also showed significant conservation of genes related to curli, biofilm, and adhesion, especially among *S.* Minnesota isolates. Genes such as csgA–G and csgD were widely detected, indicating maintenance of the central apparatus for extracellular

matrix formation and colonization. Taken together, the results suggest that the isolates studied combine antimicrobial resistance with the potential for environmental persistence and colonization, a characteristic particularly relevant in the contexts of animal production and the food chain. The phenotype–genotype correspondence is summarized in Figure 2.

3.4. Prioritization of Molecular Targets for the Structural Phase

Application of the prespecified eligibility rules prioritized CTX-M-2, CMY-2, Sul2, AcrB, and SpvC for target-specific structural assessment. AcrB and Sul2 were identical across SH23.6, SM23.7, SM23.8, and SM23.9; CMY-2 from SH23.6 and SM23.7 also showed complete sequence identity. CTX-M-2 and SpvC were associated only with SH16.3. Their coding sequences passed independent target-level completeness and reference-identity checks; however, their assignment to this isolate remains assembly derived because raw-read and orthogonal confirmation were unavailable. Tet(A) was not advanced because the present workflow did not include a membrane-embedded, target-specific binding-site protocol, while efflux was already represented by structurally tractable AcrB. InvA was retained as a genomic virulence/identification marker but was not selected as a resistance-linked structural target. These decisions follow the matrix in Table 1 and should not be interpreted as evidence against the biological importance of excluded proteins.

3.5. Correspondence Between the Target Sequence and Experimental Structures

The validation between the target sequence and the three-dimensional structure was a key quality-control component of the pipeline. The alignments between the selected bacterial proteins and the structures available in the PDB showed virtually perfect correspondence. For CMY-2, comparison with the 1ZC2 structure revealed 100.0% identity and 100.0% coverage. For Sul2, the 7S2K structure also showed 100.0% identity and full coverage. The same was true for SpvC with the 4HAH structure, again with 100.0% identity and full coverage. For AcrB, structure 6Z12 showed 99.81% identity and full coverage, with only two substitutions across 1049 residues. This result had a direct methodological implication: the CMY-2, Sul2, SpvC, and AcrB targets could be docked using experimental structures that were practically isogenic to the actual bacterial proteins. In terms of structural robustness, this scenario is clearly superior to the use of distantly related homologous models and supports the suitability to the geometry of the analyzed sites. Table 4 and Figure 3 summarize the structural correspondence supporting receptor selection.

Table 4. Prioritized targets, structural sources, validation status, and biological rationale for computational screening.

Target	Mechanistic Class	Representative Isolate	Length	Structural Source	Validation	Rationale
CTX-M-2	Class A β-lactamase	SH16.3	291 aa	ColabFold/AlphaFold2 model	100% coverage/identity; complete ORF; pLDDT 93.7; pTM 0.883	ESBL-associated target linked to β-lactam resistance
CMY-2	Class C β-lactamase	SH23.6/SM23.7	381 aa	PDB 1ZC2	100% identity; 100% coverage	AmpC β-lactamase associated with cephalosporin resistance
Sul2	Sulfonamide-resistant DHPS	SH23.6/SM23.7/SM23.8/SM23.9	271 aa	PDB 7S2K	100% identity; 100% coverage	Folate-pathway resistance target; Mg^{2+}-dependent site considered

Table 4. *Cont.*

Target	Mechanistic Class	Representative Isolate	Length	Structural Source	Validation	Rationale
AcrB	RND multidrug efflux transporter	SH23.6/SM23.7/SM23.8/SM23.9	1049 aa	PDB 6Z12	99.81% identity; 100% coverage	Highly conserved efflux target; distal pocket/hydrophobic trap selected
SpvC	Virulence effector	SH16.3	241 aa	PDB 4HAH	100% nt coverage/identity; no gaps; complete ORF; 100% protein coverage/identity to 4HAH	Virulence-associated target with phosphothreonine lyase activity

3.6. Structural Modeling of CTX-M-2 and Validation of the Predictive Model

Since no experimental structure was directly incorporated into the pipeline for the CTX-M-2 target of strain SH16.3, a predictive structure was built using ColabFold/AlphaFold2. The best model obtained was the rank_001 relaxed model, with a pLDDT of 93.7 and a pTM of 0.883, values consistent with a model of high global reliability. In addition to the global metrics, sequence inspection confirmed the presence of the catalytic motifs expected in class A β-lactamases: the SXXK motif at position 73, the SDN motif at 133–135, and the KTG motif at 237–239. The simultaneous preservation of these three functional elements reinforced the model's suitability for catalytic site-oriented docking. Thus, unlike the other targets, CTX-M-2 was docked against a predicted receptor, but with consistent evidence of structural reliability and functional conservation.

3.7. Reference-Compound Docking Results

3.7.1. Sul2 Reference-Compound Docking

The docking campaign for Sul2 revealed a methodologically significant result already in the comparison between receptors with and without the crystallographic metal. When docking was performed without retaining Mg^{2+}, some of the compounds exhibited inconsistent or unfavorable scores, including positive values for molecules that should be compatible with the functional site. In contrast, retaining the metal in the receptor (keepMG) produced a more coherent ranking from a chemical and structural standpoint. In this scenario, sulfamethoxazole was the best compound in the primary set, with −7.50 kcal/mol, followed by p-aminobenzoic acid (−7.18 kcal/mol) and sulfamethizole in the expanded set, with −7.12 kcal/mol. Other sulfonamide analogs showed intermediate or poor performance, including sulfadoxine, sulfamethazine, sulfisoxazole, sulfathiazole, dapsone, and sulfadiazine. Taken together, the results suggest that the Sul2 site was sensitive to the metal-dependent context and that the structural representation with the cofactor preserved was the most realistic option for the campaign.

3.7.2. CTX-M-2

Docking against the CTX-M-2 model yielded an even more pronounced profile for broad-spectrum cephalosporins. Ceftriaxone was the best ligand, with −8.61 kcal/mol, followed by cefepime (−8.08 kcal/mol) and cefotaxime (−8.07 kcal/mol). Next came ampicillin (−7.70 kcal/mol), aztreonam (−7.60 kcal/mol), and avibactam (−7.19 kcal/mol). Compounds such as amoxicillin, ceftazidime, clavulanic acid, tazobactam, and sulbactam performed less well. This result was particularly interesting because it reinforced the functional relevance of CTX-M-2 as a target associated with extended-spectrum β-lactam

resistance in the SH16.3 isolate. Although docking does not replace kinetic assays, the observed pattern was consistent with strong structural recognition of cephalosporins by the modeled catalytic site.

3.7.3. SpvC

For the virulence effector SpvC, the best results were obtained with phosphorylated or phosphonated compounds that are structurally compatible with the type of chemistry recognized by this protein. The best score was observed for O-phospho-L-tyrosine (−6.25 kcal/mol), followed by phenylphosphonic acid (−5.31 kcal/mol) and 4-nitrophenyl phosphate (−5.22 kcal/mol). Other compounds in the set, such as O-phospho-L-threonine, O-phospho-L-serine, glyphosate, fosfomycin, phosphonoacetic acid, and phosphonoformate, exhibited less favorable scores. These data support the plausibility of the chosen site and indicate that the target preferentially responds to ligands containing phosphorylated groups or phosphorous mimetics, consistent with its functional nature.

3.7.4. AcrB Reference-Compound Docking

The AcrB target exhibited one of the most promising profiles in the primary screening. In the distal pocket, the best compound in the reference set was phenylalanine-arginine β-naphthylamide (PAβN), with −8.67 kcal/mol, followed by doxycycline (−8.50 kcal/mol) and tetracycline (−7.80 kcal/mol). Tigecycline showed −7.19 kcal/mol, while minocycline, chloramphenicol, ciprofloxacin, florfenicol, norfloxacin, and nalidixic acid exhibited less favorable values. This ranking is important for two reasons. First, it showed that the distal pocket defined for docking was capable of recognizing molecules known to be associated with transport, efflux, or functional modulation of the system. Second, it provided a solid baseline for the optimization step using analogs, allowing direct comparison between the parent compounds and the derivatives generated in RDKit. The comparative docking profile across targets is summarized in Figure 4.

3.8. Computational Analog Generation and Reprioritization for Sul2 and AcrB

3.8.1. Sul2

The library of Sul2 analogs generated by RDKit yielded a reduced set of valid candidates, of which 95 passed internal filters after prioritization. The best compounds ranked by cheminformatics profile included sulfamethazine, sulfamethizole, sulfisoxazole, sulfamethoxazole, and the derivative BRICS_00001. However, when these compounds were redocked on the same Sul2 receptor, the structural gain was limited.

The best scores were −7.50 kcal/mol for sulfamethizole and −7.44 kcal/mol for sulfamethoxazole, followed by sulfisoxazole (−7.02 kcal/mol). The BRICS-derived candidate BRICS_00001 had a substantially less favorable score (−4.43 kcal/mol), and sulfamethazine scored −3.36 kcal/mol. Thus, the analog-generation step on Sul2 did not yield a derivative superior to the best parent compounds. Figure 9 presents the verified structures of the principal parent compounds and the corresponding redocking comparison. BRICS_00001 is retained as a score-only entry because its source SMILES/SDF was not available in the archived assets used for this revision.

3.8.2. AcrB

The AcrB campaign generated 234 valid molecules, of which 95 passed the operational filters. Several analogs received numerically more favorable GNINA scores than the parent compounds under the same receptor and docking settings. The most favorable scores were obtained for ACRB_BRICS_00197 (−10.99 kcal/mol), ACRB_BRICS_00124 (−10.80 kcal/mol), and ACRB_BRICS_00089 (−10.33 kcal/mol), followed by ACRB_BRICS_00076, ACRB_BRICS_00115, and ACRB_BRICS_00206 (−9.65 kcal/mol each). These nu-

merical differences do not establish improved affinity or biological activity. PLIP provided additional pose-level support for ACRB_BRICS_00124 (6 hydrogen bonds, 3 hydrophobic contacts, and 1 salt bridge), ACRB_BRICS_00076 (5 hydrogen bonds and 8 hydrophobic contacts), ACRB_BRICS_00206 (4 hydrogen bonds, 4 hydrophobic contacts, and 1 π-stacking interaction), and ACRB_BRICS_00115 (3 hydrogen bonds, 3 hydrophobic contacts, and 1 π-stacking interaction). Recurring pocket-associated residues included Asn81, Gln89, Ser133, Ser134, Phe615, Phe617, Glu673, and Asn719. Under the integrated computational ranking, ACRB_BRICS_00124 was the highest-priority candidate for further evaluation. Figures 6–8 and Table 5 summarize the AcrB results, while Figure 9 summarizes the Sul2 comparison.

Table 5. Integrated computational ranking of AcrB BRICS analogs based on GNINA score and PLIP-supported interaction profiles.

Compound	GNINA Score (kcal/mol)	H-Bonds	Hydrophobic Contacts	Salt Bridge	π-Stacking	Integrated Assessment
ACRB_BRICS_00124	−10.80	6	3	1	0	Leading candidate; favorable score and extensive interaction network
ACRB_BRICS_00076	−9.65	5	8	0	0	Strong hydrophobic accommodation and multiple hydrogen bonds
ACRB_BRICS_00206	−9.65	4	4	0	1	Balanced interaction profile with π-stacking support
ACRB_BRICS_00115	−9.65	3	3	0	1	Favorable score with moderate PLIP-supported interactions
ACRB_BRICS_00197	−10.99	0	0	0	0	Top GNINA score; no PLIP contacts detected in the selected pose
ACRB_BRICS_00089	−10.33	0	0	0	0	Favorable GNINA score; no PLIP contacts detected in the selected pose

ACRB_BRICS_00197 and ACRB_BRICS_00089 received highly favorable GNINA scores, but PLIP did not recover explicit noncovalent contacts for their selected poses. These candidates were therefore classified as lower-confidence score-driven results rather than prioritized hits. This discordance illustrates why docking scores should not be interpreted independently of pose inspection, interaction profiling, receptor flexibility, solvation, and experimental evidence.

3.9. Integration of Phenotype, Genomics, and Molecular Prioritization

When analyzed together, the results indicate overall consistency between the experimental behavior of the strains, the detected genetic content, and the structural prioritization of targets. The multidrug susceptibility testing provided the phenotypic background. Genomics revealed biologically plausible combinations of genes associated with resistance to β-lactams, sulfonamides, and tetracyclines, as well as efflux systems and persistence genes. Sequence–structure validation showed that the prioritized targets were anchored to experimental receptors virtually identical to the actual bacterial proteins or, in the case of CTX-M-2, to a highly reliable model.

At the functional level, the computational results identified two patterns. For Sul2, the tested BRICS chemical space did not produce analog scores clearly more favorable than the best parental compounds. For AcrB, several generated analogs received numerically more favorable scores and some poses also recovered coherent PLIP interaction profiles. This comparison supports prioritizing selected AcrB complexes for additional computational and experimental assessment, but it does not establish improved affinity, pump inhibition, antibacterial activity, or drug candidacy.

This difference between the targets is, in itself, an important finding. Rather than forcing a uniform narrative for all proteins, the data indicate that the chemical space explored was more responsive in the distal pocket of AcrB, whereas Sul2 exhibited more restrictive structural behavior. Consequently, the results obtained justify prioritizing the best AcrB complexes for the next stages of structural refinement, including molecular dynamics and a more in-depth evaluation of the conformational stability of protein–ligand recognition.

4. Discussion

The results of this study reinforce the notion that the emergence and persistence of *Salmonella* Heidelberg and *Salmonella* Minnesota in the Brazilian poultry industry should not be interpreted solely as epidemiological phenomena related to serovar frequency, but rather as the expression of strains adapted to intensive production environments, frequently associated with multidrug resistance and genetic profiles compatible with persistence and dissemination. On a broader scale, genomic analyses have demonstrated that *S.* Heidelberg and *S.* Minnesota are among the most relevant serovars in chickens produced in Brazil and in Brazilian poultry products detected abroad, suggesting adaptive success and a potential public health impact beyond the local context [2].

The convergence between phenotype and genotype was one of the strongest findings of the study. The detection of blaCTX-M-2, blaCMY-2, sul1/sul2, tet(A), and components of the AcrAB-TolC system provides a mechanistically plausible explanation for the resistance profiles observed in the antibiogram, especially against β-lactams, sulfonamides, tetracyclines, and fluoroquinolones. This pattern is consistent with Brazilian studies that identified, in *S.* Heidelberg and *S.* Minnesota of avian origin, the predominance of blaCMY-2, frequently associated with IncC plasmids, as well as combinations of genes that support multidrug phenotypes and increase the potential for horizontal spread of resistance [3]. Converging data from national surveys have shown high and increasing rates of resistance among *Salmonella* isolates from chicken meat in Brazil, particularly among the Heidelberg and Minnesota serovars [40].

SH16.3 must be interpreted as a technical outlier rather than as evidence of greater biological complexity. Its unexpectedly large assembled size of 4432 contigs and N50 of 4160 bp cannot distinguish contamination, a mixed template, uneven read support, a repetitive sequence, or an assembly artifact from genuine accessory-genome content. Accordingly, the assembly was not used for genome-wide comparative inference. Independent reanalysis showed that the *blaCTX-M-2* and *spvC* coding sequences were complete and exact matches to curated references, reducing concern about truncation or contig-edge artifacts. Nevertheless, these findings remain assembly derived and cannot exclude contamination or mixed-template origin without raw-read support or orthogonal confirmation. This conservative treatment prevents the low-quality assembly from being used to support claims regarding mobilome expansion, plasmid content, or genomic rearrangement.

Another strength of the study was the sequence–structure validation. For CMY-2, Sul2, SpvC, and AcrB, the near-perfect correspondence between the proteins extracted from the isolates and the experimental structures selected from the PDB substantially reduces one of the main sources of uncertainty in docking studies: the use of receptors that are structurally

distant from the actual sequence of the target organism. This aspect strengthens the internal interpretation of the screening campaigns, as it brings the computational system closer to the molecular reality of the studied isolates. For CTX-M-2, although it was necessary to employ a predictive model, the high pLDDT and pTM values, combined with the preservation of the classic catalytic motifs of class A β-lactamases, support the model's suitability for initial exploration of the active site. Nevertheless, in accordance with the standards of rigor expected by high-impact journals, it is important to recognize that even high-quality models do not replace experimental structural validation, especially when subtle differences in geometry can influence ligand pose and binding affinity. SpvC is a Salmonella type III-secreted effector with phosphothreonine lyase activity toward host MAPKs, supporting the mechanistic relevance of its catalytic cavity; however, isolate-level provenance of the SH16.3 locus remains assembly derived [41,42].

In the case of Sul2, the results highlight a methodologically relevant observation: maintaining Mg^{2+} at the functional site produced more consistent rankings than the version without the cofactor. This result suggests that the receptor's metal-dependent environment directly influences ligand binding and recognition, which is consistent with the fact that small changes in the site representation can significantly alter docking scores. Although sulfamethoxazole and some analogs exhibited relatively favorable performance, the chemical expansion stage did not yield derivatives clearly superior to the parent compounds. In interpretive terms, this suggests that the chemical space explored for Sul2 was more restrictive, or that the initial set of fragments and seeds was not sufficiently diverse to break the recognition pattern already established by the target. Thus, the data support Sul2 as a biologically relevant target, but do not indicate, at this stage, a strong axis of structural optimization comparable to that observed for AcrB.

AcrB emerged as the highest-priority computational axis in the present dataset, from both biological and cheminformatics perspectives. This interpretation is supported by three converging lines of evidence. First, AcrB was detected in multiple isolates with a highly conserved sequence, indicating that the target represents a stable trait of the bacterial population analyzed. Second, the distal pocket/hydrophobic trap selected for docking is recognized in the literature as a critical region for the development of RND pump inhibitors, including the interaction of compounds in this phenylalanine-rich cavity [43,44]. Third, the BRICS-based analog generation step produced compounds with numerically more favorable scores relative to the parent compounds, and some of these candidates also showed plausible interaction support via PLIP. In particular, ACRB_BRICS_00124, ACRB_BRICS_00076, and ACRB_BRICS_00206 combined favorable scores with coherent networks of hydrogen bonds, hydrophobic contacts, and, in some cases, π interactions, suggesting consistent occupation of the prioritized functional region. In a broader context, these findings are consistent with the renewed interest in efflux inhibitors for Gram-negative bacteria, as RND pumps remain among the primary drivers of multidrug resistance and continue to be targets of high strategic value [9,10,44].

Nevertheless, the interpretation of docking results should remain deliberately conservative. Docking scores, even in neural network-enhanced engines such as GNINA, do not equate to experimental affinities and may overestimate certain poses when the receptor representation, conformational flexibility, solvation, and system dynamics are not fully captured. Recent studies emphasize that deep learning-based docking and scoring methods expand screening capabilities but still exhibit significant limitations regarding generalization, calibration, and experimental translation. Thus, the fact that two compounds with excellent scores in AcrB did not produce explicit interactions in PLIP is a pertinent methodological caveat, not a contradiction. In practice, this means that the energy ranking should be interpreted in conjunction with the pose, chemical consistency, recoverability of

interactions, and, ideally, subsequent refinement steps, such as molecular dynamics and phenotypic validation.

From a translational perspective, the study also clearly illustrates the current role of WGS as a platform for functional prioritization, rather than merely descriptive surveillance. Recent reviews highlight that whole-genome sequencing has revolutionized outbreak investigation and the characterization of foodborne pathogens by integrating typing, traceability, and genetic profiles of resistance and virulence. In this sense, the strategy adopted here, starting from the phenotype, integrating genomics, reducing protein redundancy, validating the structural suitability of targets, and only then proceeding to molecular screening, represents a robust analytical framework well aligned with current trends in applied genomic microbiology [7]. The fact that different targets responded differently to chemical screening is also relevant, as it shows that the integration of molecular epidemiology and cheminformatics can identify, even at an early stage, which pathways warrant greater experimental investment.

In summary, the data obtained support three main conclusions. First, the analyzed isolates fit into the contemporary landscape of multidrug-resistant poultry *Salmonella* in Brazil, especially regarding the importance of *S.* Heidelberg and *S.* Minnesota as reservoirs of resistance genes and persistence traits [2,4–6]. Second, the consistency between the antibiogram, genetic content, and structural prioritization confirms the utility of an integrative approach for the rational selection of targets. Third, among the proteins investigated, AcrB stood out as the target most responsive to chemoinformatic optimization, while Sul2 exhibited more conservative behavior and CTX-M-2 and SpvC remained biologically relevant targets, though still dependent on further experimental and structural investigation. Thus, the central contribution of this study is not to claim the discovery of ready-to-use inhibitors, but to demonstrate, based on consistent genomic and structural evidence, a rational pathway for prioritizing targets and molecular candidates in multidrug-resistant avian strains of *Salmonella*.

Limitations

This study is exploratory and predominantly computational. No candidate molecule was synthesized or tested for AcrB inhibition, antibacterial activity, toxicity, selectivity, or synergy with antimicrobials. Single-structure docking and PLIP interaction recovery do not account fully for receptor flexibility, protonation uncertainty, explicit solvation, membrane context, transport-cycle conformations, or binding kinetics. Molecular dynamics, ensemble/flexible-receptor docking, and end-point free-energy approaches such as MM-GBSA/MM-PBSA were not performed. BRICS-derived structures were not evaluated for synthetic accessibility, chemical stability, metabolic liability, target selectivity, or experimental feasibility. In addition, SH16.3 had a severely fragmented assembly. Target-level analyses supported complete blaCTX-M-2 and spvC coding sequences, but raw-read mapping and orthogonal PCR/Sanger confirmation or resequencing were not available; therefore, the locus assignments remain assembly derived. These limitations restrict the conclusions to virtual screening and computational prioritization.

5. Conclusions

The integration of phenotypic susceptibility data, whole-genome sequencing, explicit target-eligibility rules, sequence–structure validation, target-specific docking, and interaction profiling provided a reproducible framework for computational prioritization in multidrug-resistant poultry-associated *Salmonella enterica*. AcrB was conserved among four selected isolates and yielded the strongest combined numerical docking and PLIP-supported profiles within the chemical space tested, whereas Sul2 did not show a clear

analog-prioritization improvement. Findings involving CTX-M-2 and SpvC from SH16.3 are supported at the coding-sequence level but remain limited by uncertain isolate-level provenance due to the poor assembly quality and lack of raw-read and orthogonal confirmation. The study does not demonstrate target discovery, drug discovery, binding affinity, or antimicrobial activity. The prioritized AcrB candidates should therefore be regarded as hypotheses for molecular-dynamics refinement, synthetic-feasibility assessment, and experimental validation.

Author Contributions: J.P.T.: conceptualization, methodology, formal analysis, investigation, data curation, visualization, writing—original draft, and writing—review and editing. D.F.d.L.N.: methodology, genomic and structural analysis support, data interpretation, and writing—review and editing. C.A.B.: investigation, data interpretation, and writing—review and editing. M.M.B.: supervision, project administration, resources, and writing—review and editing. P.F.d.S.T.: investigation, microbiological support, and writing—review and editing. R.S.d.S.: data analysis support, interpretation, and writing—review and editing. S.K.: structural biology and cheminformatics interpretation, software support, and writing—review and editing. T.Q.F.: isolate provision, microbiological interpretation, validation, resources, and writing—review and editing. L.d.C.M.S.: supervision, resources, project administration, and writing—review and editing. All authors critically reviewed the manuscript for important intellectual content, approved the final version for publication, and agree to be accountable for all aspects of the work, including the accuracy and integrity of their own contributions and the appropriate investigation and resolution of questions concerning any part of the manuscript. All authors have read and agreed to the published version of the manuscript.

Funding: This work was partially supported by the Conselho Nacional de Desenvolvimento Científico e Tecnológico (CNPq), Brazil, process no. 315893/2023-0, awarded to Lenita de Cássia Moura Stefani. Support for the article processing charge was requested through the PRODIP Call of the Center for Distance Education (CEAD), State University of Santa Catarina (UDESC).

Institutional Review Board Statement: Not applicable. This study used archived bacterial isolates obtained from routine poultry-production surveillance and did not involve human participants or experimental procedures with live animals.

Informed Consent Statement: Not applicable.

Data Availability Statement: Processed datasets and reproducibility materials, including resistance-profile tables, assembly metrics, screening outputs, target sequences, docking-score tables, BRICS-derived descriptors, PLIP summaries, figure-source data, and custom scripts, are available in the public GitHub repository: https://github.com/BioinformaticaUDESC/salmonella-structure-pipeline- (accessed on 12 September 2026). The five draft genome assemblies have been submitted to NCBI GenBank under genome submission SUB16387240. BioProject, BioSample, and WGS accession numbers are pending NCBI processing and will be added upon assignment. Raw whole-genome sequencing reads will be deposited in the NCBI Sequence Read Archive before publication.

Acknowledgments: Chemical structures were independently generated from validated SMILES using RDKit. The authors take full responsibility for the content of the manuscript. The authors also acknowledge the PRODIP Call of CEAD/UDESC for institutional support related to publication funding.

Conflicts of Interest: The authors declare no conflicts of interest.

References

1. World Health Organization (WHO). *Salmonella (Non-Typhoidal)*; WHO: Geneva, Switzerland, 2018. Available online: https://www.who.int/news-room/fact-sheets/detail/salmonella-(non-typhoidal) (accessed on 4 August 2026).
2. Alikhan, N.-F.; Moreno, L.Z.; Castellanos, L.R.; Chattaway, M.A.; McLauchlin, J.; Lodge, M.; O'gRady, J.; Zamudio, R.; Doughty, E.; Petrovska, L.; et al. Dynamics of Salmonella enterica and antimicrobial resistance in the Brazilian poultry industry and global impacts on public health. *PLoS Genet.* **2022**, *18*, e1010174. [CrossRef] [PubMed]

3. Saidenberg, A.B.S.; Franco, L.S.; Reple, J.N.; Hounmanou, Y.M.G.; Casas, M.R.T.; Cardoso, B.; Esposito, F.; Lincopan, N.; Dalsgaard, A.; Stegger, M.; et al. *Salmonella* Heidelberg and *Salmonella* Minnesota in Brazilian broilers: Genomic characterization of third-generation cephalosporin and fluoroquinolone-resistant strains. *Environ. Microbiol. Rep.* **2023**, *15*, 119–128. [CrossRef] [PubMed]
4. Figueira, A.d.A.; Dias, T.S.; Costa, G.A.; Abreu, D.L.d.C.; Medeiros, L.d.S.; Pereira, V.L.d.A. Phenotypic and Genomic Assessment of Antimicrobial Resistance and Virulence Factors Determinants in *Salmonella* Heidelberg Isolated from Broiler Chickens. *Animals* **2025**, *15*, 1003. [CrossRef] [PubMed]
5. Mesa, D.; Almeida, S.; Krul, D.; Vasconcelos, T.M.; Siqueira, A.C.; Negoseki, B.R.d.S.; de Sousa, I.; Cardoso, R.; Conte, D.; Dalla-Costa, L.M. An insight into the characterization of multidrug resistant Salmonella Minnesota isolated from poultry in Brazil. *Infect. Genet. Evol.* **2026**, *139*, 105896. [CrossRef] [PubMed]
6. Justino, L.; Baptista, A.A.S.; de Carvalho, R.H.; Casella, T.; Sano, E.L.; Costa, J.V.d.S.; da Costa, A.R.; Menck-Costa, M.F.; Pilli, M.F.M.; Benteo, A.C.B.; et al. Environmental Persistence and Genotypic and Phenotypic Characterization of *Salmonella* Minnesota in Poultry Slaughterhouses. *Pathogens* **2026**, *15*, 247. [CrossRef] [PubMed]
7. Gomes, E.; Araújo, D.; Nogueira, T.; Oliveira, R.; Silva, S.; Oliveira, L.V.N.; Azevedo, N.F.; Almeida, C.; Castro, J. Advances in whole genome sequencing for foodborne pathogens: Implications for clinical infectious disease surveillance and public health. *Front. Cell. Infect. Microbiol.* **2025**, *15*, 1593219. [CrossRef] [PubMed]
8. European Food Safety Authority (EFSA). *Whole Genome Sequencing in Foodborne Outbreaks*; EFSA: Parma, Italy, 2026. Available online: https://www.efsa.europa.eu/en/topics/topic/whole-genome-sequencing-foodborne-outbreaks (accessed on 4 August 2026).
9. El-Demerdash, A.S.; Kamel, S.A.; Elariny, E.Y.T.; Henidi, H.; Mahran, Y.; Alahdal, H.; Saleh, A.M.; Ibrahim, R.A. Natural Inhibitors of *Salmonella* MDR Efflux Pumps AcrAB and AcrD: An Integrated In Silico, Molecular, and In Vitro Investigation. *Int. J. Mol. Sci.* **2024**, *25*, 12949. [CrossRef] [PubMed]
10. Schuster, S.; Vavra, M.; Wirth, D.A.N.; Kern, W.V. Comparative reassessment of AcrB efflux inhibitors reveals differential impact of specific pump mutations on the activity of potent compounds. *Microbiol. Spectr.* **2024**, *12*, e0304523. [CrossRef] [PubMed]
11. Magiorakos, A.-P.; Srinivasan, A.; Carey, R.B.; Carmeli, Y.; Falagas, M.E.; Giske, C.G.; Harbarth, S.; Hindler, J.F.; Kahlmeter, G.; Olsson-Liljequist, B.; et al. Multidrug-resistant, extensively drug-resistant and pandrug-resistant bacteria: An international expert proposal for interim standard definitions for acquired resistance. *Clin. Microbiol. Infect.* **2012**, *18*, 268–281. [CrossRef] [PubMed]
12. Sambrook, J.; Russell, D.W. *Molecular Cloning: A Laboratory Manual*, 3rd ed.; Cold Spring Harbor Laboratory Press: Cold Spring Harbor, NY, USA, 2001.
13. Thermo Fisher Scientific. *Assessment of Nucleic Acid Purity*; Technical Note TN52646-E-0215M; Thermo Fisher Scientific: Wilmington, DC, USA, 2015.
14. Chen, S.; Zhou, Y.; Chen, Y.; Gu, J. fastp: An ultra-fast all-in-one FASTQ preprocessor. *Bioinformatics* **2018**, *34*, i884–i890. [CrossRef] [PubMed]
15. Bankevich, A.; Nurk, S.; Antipov, D.; Gurevich, A.A.; Dvorkin, M.; Kulikov, A.S.; Lesin, V.M.; Nikolenko, S.I.; Pham, S.; Prjibelski, A.D.; et al. SPAdes: A new genome assembly algorithm and its applications to single-cell sequencing. *J. Comput. Biol.* **2012**, *19*, 455–477. [CrossRef] [PubMed]
16. Wick, R.R.; Schultz, M.B.; Zobel, J.; Holt, K.E. Bandage: Interactive visualization of *de novo* genome assemblies. *Bioinformatics* **2015**, *31*, 3350–3352. [CrossRef] [PubMed]
17. Shen, W.; Le, S.; Li, Y.; Hu, F. SeqKit: A cross-platform and ultrafast toolkit for FASTA/Q file manipulation. *PLoS ONE* **2016**, *11*, e0163962. [CrossRef] [PubMed]
18. Hyatt, D.; Chen, G.-L.; Locascio, P.F.; Land, M.L.; Larimer, F.W.; Hauser, L.J. Prodigal: Prokaryotic gene recognition and translation initiation site identification. *BMC Bioinform.* **2010**, *11*, 119. [CrossRef] [PubMed]
19. Feldgarden, M.; Brover, V.; Gonzalez-Escalona, N.; Frye, J.G.; Haendiges, J.; Haft, D.H.; Hoffmann, M.; Pettengill, J.B.; Prasad, A.B.; Tillman, G.E.; et al. AMRFinderPlus and the reference gene catalog facilitate examination of the genomic links among antimicrobial resistance, stress response, and virulence. *Sci. Rep.* **2021**, *11*, 12728. [CrossRef] [PubMed]
20. Chen, L.; Yang, J.; Yu, J.; Yao, Z.; Sun, L.; Shen, Y.; Jin, Q. VFDB: A reference database for bacterial virulence factors. *Nucleic Acids Res.* **2005**, *33*, D325–D328. [CrossRef] [PubMed]
21. Jia, B.; Raphenya, A.R.; Alcock, B.; Waglechner, N.; Guo, P.; Tsang, K.K.; Lago, B.A.; Dave, B.M.; Pereira, S.; Sharma, A.N.; et al. CARD 2017: Expansion and model-centric curation of the comprehensive antibiotic resistance database. *Nucleic Acids Res.* **2017**, *45*, D566–D573. [CrossRef] [PubMed]
22. Zankari, E.; Hasman, H.; Cosentino, S.; Vestergaard, M.; Rasmussen, S.; Lund, O.; Aarestrup, F.M.; Larsen, M.V. Identification of acquired antimicrobial resistance genes. *J. Antimicrob. Chemother.* **2012**, *67*, 2640–2644. [CrossRef] [PubMed]
23. Gupta, S.K.; Padmanabhan, B.R.; Diene, S.M.; Lopez-Rojas, R.; Kempf, M.; Landraud, L.; Rolain, J.-M. ARG-ANNOT, a new bioinformatic tool to discover antibiotic resistance genes in bacterial genomes. *Antimicrob. Agents Chemother.* **2014**, *58*, 212–220. [CrossRef] [PubMed]

24. Lakin, S.M.; Dean, C.; Noyes, N.R.; Dettenwanger, A.; Ross, A.S.; Doster, E.; Rovira, P.; Abdo, Z.; Jones, K.L.; Ruiz, J.; et al. MEGARes: An antimicrobial resistance database for high throughput sequencing. *Nucleic Acids Res.* **2017**, *45*, D574–D580. [CrossRef] [PubMed]
25. Carattoli, A.; Zankari, E.; Garcìa-Fernandez, A.; Larsen, M.; Lund, O.; Voldby Villa, L.; Møller Aarestrup, F.; Hasman, H. In Silico detection and typing of plasmids using PlasmidFinder and plasmid multilocus sequence typing. *Antimicrob. Agents Chemother.* **2014**, *58*, 3895–3903. [CrossRef] [PubMed]
26. Robertson, J.; Nash, J.H.E. MOB-suite: Software tools for clustering, reconstruction and typing of plasmids from draft assemblies. *Microb. Genom.* **2018**, *4*, e000206. [CrossRef] [PubMed]
27. Buchfink, B.; Reuter, K.; Drost, H.-G. Sensitive protein alignments at tree-of-life scale using DIAMOND. *Nat. Methods* **2021**, *18*, 366–368. [CrossRef] [PubMed]
28. Pal, C.; Bengtsson-Palme, J.; Rensing, C.; Kristiansson, E.; Larsson, D.G.J. BacMet: Antibacterial biocide and metal resistance genes database. *Nucleic Acids Res.* **2014**, *42*, D737–D743. [CrossRef] [PubMed]
29. Schwengers, O.; Jelonek, L.; Dieckmann, M.A.; Beyvers, S.; Blom, J.; Goesmann, A. Bakta: Rapid and standardized annotation of bacterial genomes via alignment-free sequence identification. *Microb. Genom.* **2021**, *7*, 000685. [CrossRef] [PubMed]
30. Mirdita, M.; Schütze, K.; Moriwaki, Y.; Heo, L.; Ovchinnikov, S.; Steinegger, M. ColabFold: Making protein folding accessible to all. *Nat. Methods* **2022**, *19*, 679–682. [CrossRef] [PubMed]
31. Jumper, J.; Evans, R.; Pritzel, A.; Green, T.; Figurnov, M.; Ronneberger, O.; Tunyasuvunakool, K.; Bates, R.; Žídek, A.; Potapenko, A.; et al. Highly accurate protein structure prediction with AlphaFold. *Nature* **2021**, *596*, 583–589. [CrossRef] [PubMed]
32. Kim, S.; Chen, J.; Cheng, T.; Gindulyte, A.; He, J.; He, S.; Li, Q.; Shoemaker, B.A.; Thiessen, P.A.; Yu, B.; et al. PubChem 2025 update. *Nucleic Acids Res.* **2025**, *53*, D1516–D1525. [CrossRef] [PubMed]
33. McNutt, A.T.; Francoeur, P.; Aggarwal, R.; Masuda, T.; Meli, R.; Ragoza, M.; Sunseri, J.; Koes, D.R. GNINA 1.0: Molecular docking with deep learning. *J. Cheminform.* **2021**, *13*, 43. [CrossRef] [PubMed]
34. Trott, O.; Olson, A.J. AutoDock Vina: Improving the speed and accuracy of docking with a new scoring function, efficient optimization, and multithreading. *J. Comput. Chem.* **2010**, *31*, 455–461. [CrossRef] [PubMed]
35. RDKIT. RDKit: Open-source cheminformatics. Release 2024_09_2. *Zenodo* **2024**. [CrossRef]
36. Degen, J.; Wegscheid-Gerlach, C.; Zaliani, A.; Rarey, M. On the art of compiling and using 'drug-like' chemical fragment spaces. *ChemMedChem* **2008**, *3*, 1503–1507. [CrossRef] [PubMed]
37. Rappe, A.K.; Casewit, C.J.; Colwell, K.S.; Goddard, W.A.; Skiff, W.M. UFF, a full periodic table force field for molecular mechanics and molecular dynamics simulations. *J. Am. Chem. Soc.* **1992**, *114*, 10024–10035. [CrossRef]
38. Bickerton, G.R.; Paolini, G.V.; Besnard, J.; Muresan, S.; Hopkins, A.L. Quantifying the chemical beauty of drugs. *Nat. Chem.* **2012**, *4*, 90–98. [CrossRef] [PubMed]
39. Salentin, S.; Schreiber, S.; Haupt, V.J.; Adasme, M.F.; Schroeder, M. PLIP: Fully automated protein–ligand interaction profiler. *Nucleic Acids Res.* **2015**, *43*, W443–W447. [CrossRef] [PubMed]
40. Rau, R.B.; Ribeiro, A.R.; dos Santos, A.; Barth, A.L. Antimicrobial resistance of *Salmonella* from poultry meat in Brazil: Results of a nationwide survey. *Epidemiol. Infect.* **2021**, *149*, e228. [CrossRef]
41. Mazurkiewicz, P.; Thomas, J.; Thompson, J.A.; Liu, M.; Arbibe, L.; Sansonetti, P.; Holden, D.W. SpvC is a *Salmonella* effector with phosphothreonine lyase activity on host mitogen-activated protein kinases. *Mol. Microbiol.* **2008**, *67*, 1371–1383. [CrossRef] [PubMed]
42. Li, H.; Xu, H.; Zhou, Y.; Zhang, J.; Long, C.; Li, S.; Chen, S.; Zhou, J.-M.; Shao, F. The phosphothreonine lyase activity of a bacterial type III effector family. *Science* **2007**, *315*, 1000–1003. [CrossRef] [PubMed]
43. Aron, Z.; Opperman, T.J. The hydrophobic trap—The Achilles heel of RND efflux pumps. *Res. Microbiol.* **2018**, *169*, 393–400. [CrossRef] [PubMed]
44. Duffey, M.; Jumde, R.P.; da Costa, R.M.; Ropponen, H.-K.; Blasco, B.; Piddock, L.J. Extending the Potency and Lifespan of Antibiotics: Inhibitors of Gram-Negative Bacterial Efflux Pumps. *ACS Infect. Dis.* **2024**, *10*, 1458–1482. [CrossRef] [PubMed]

Disclaimer/Publisher's Note: The statements, opinions and data contained in all publications are solely those of the individual author(s) and contributor(s) and not of MDPI and/or the editor(s). MDPI and/or the editor(s) disclaim responsibility for any injury to people or property resulting from any ideas, methods, instructions or products referred to in the content.